

Magnetism and Superconductivity in the Two-Dimensional 16-Band d-p Model for Iron-Based Superconductors

Yuki Yanagi, Youichi Yamakawa and Yoshiaki Ono

Department of Physics, Niigata University, Ikarashi, Niigata 950-2181, Japan

The electronic states of the Fe_2As_2 plane in iron-based superconductors are investigated on the basis of the two-dimensional 16-band d-p model which includes the Coulomb interaction on a Fe site: the intra- and inter-orbital direct terms U and U^0 , the Hund's coupling J and the pair-transfer J^0 . Using the random phase approximation (RPA), we obtain the magnetic phase diagram including the stripe and the incommensurate order on the U^0 - J plane. We also solve the superconducting gap equation within the RPA and find that, for large J , the most favorable pairing symmetry is extended s-wave whose order parameter changes its sign between the hole pockets and the electron pockets, while it is d_{xy} -wave for small J .

KEYWORDS: iron-based superconductors, 16-band d-p model, pairing symmetry, RPA, Hund's coupling

The newly discovered iron-based superconductors^{1,2)} $\text{RFePnO}_{1-x}\text{Fx}$ ($\text{R} = \text{Rare Earth}, \text{Pn} = \text{As, P}$) with a transition temperature up to $T_c = 55\text{K}$ ³⁾ have attracted much attention. The Fe-nondoped samples exhibit the stripe-type antiferromagnetic order with a transition temperature 134K and a magnetic moment $0.36\mu_B$ ⁴⁾ at low temperature. With increasing F-doping, the system becomes metallic and the antiferromagnetic order disappears,²⁾ and then, the superconductivity emerges for $x = 0.11$ with $T_c = 26\text{K}$. Specific features of the systems are two-dimensionality of the conducting Fe_2As_2 plane and the orbital degrees of freedom in Fe^{2+} ($3d^6$).^{1,2)} The pairing symmetry together with the mechanism of the superconductivity is one of the most significant issues.

The NMR Knight shift measurements revealed that the superconductivity of the systems is the spin-singlet pairing.^{5,6)} Fully gapped superconducting states have been predicted by various experiments such as the penetration depth,⁷⁾ the specific heat,⁸⁾ the angle resolved photoemission spectroscopy (ARPES)⁹⁽¹¹⁾ and the impurity effect on T_c .⁶⁾ In contrast to the above mentioned experiments, the NMR relaxation rate shows the power law behavior $1/T_1 \propto T^3$ below T_c ,¹²⁾ suggesting the superconducting gaps with line nodes.

Theoretically, the first principle calculations have predicted that the nondoped system is metallic with two or three concentric hole Fermi surfaces around ($k = (0;0)$) point and two elliptical electron Fermi surfaces around M ($k = (\pi; \pi)$) point.¹³⁽¹⁶⁾ Mazin et al. suggested that the spin-singlet extended s-wave pairing whose order parameter changes its sign between the hole pockets and the electron pockets is favored due to the antiferromagnetic spin fluctuations.^{17,18)} According to the weak coupling approaches based on multi-orbital Hub-

bard models,¹⁹⁽²²⁾ the extended s-wave pairing or the d_{xy} -wave pairing is expected to emerge. The details of the band structure and the Fermi surface are crucial for determining the pairing symmetry. Therefore, theoretical studies based on a more realistic model which includes both the Fe 3d orbitals and the As 4p orbitals, so called d-p model, are highly desired.

In the previous paper,²³⁾ we have investigated the pairing symmetry of the two-dimensional 16-band d-p model by using the random phase approximation (RPA). It has been found that, for a larger value of $J=U^0$, the most favorable pairing symmetry is extended s-wave, while, for a smaller value of $J=U^0$, it is d_{xy} -wave. However, the detailed electronic states in the whole parameter region of U^0 and J have not been discussed there. The purpose of this paper is to obtain the detailed phase diagram including the magnetism and the superconductivity in the U^0 - J plane.

First of all, we perform the density functional calculation for LaFeAsO with the generalized gradient approximation of Perdew, Burke and Ernzerhof²⁴⁾ by using the WIEN2k package,²⁵⁾ where the lattice parameters ($a = 4.03268\text{\AA}$, $c = 8.74111\text{\AA}$) and the internal coordinates ($z_{\text{La}} = 0.14134$, $z_{\text{As}} = 0.65166$) are experimentally determined.²⁶⁾ Considering that there are two distinct Fe and As sites in the crystallographic unit cell, we then derive the two-dimensional 16-band d-p model,^{23,27)} where 3d orbitals ($d_{3z^2-r^2}$, $d_{x^2-y^2}$, d_{xy} , d_{yz} , d_{zx}) of two Fe atoms ($\text{Fe}^1 = \text{A}$, $\text{Fe}^2 = \text{B}$) and 4p orbitals (p_x , p_y , p_z) of two As atoms are explicitly included. We note that x ; y axes are rotated by 45 degrees from the direction along Fe-Fe bonds. The noninteracting part of the d-p model is given by the following tight-binding Hamiltonian,

$$H_0 = \sum_{i,j} \sum_{\sigma} t_{ij}^{\sigma} c_{i\sigma}^{\dagger} c_{j\sigma} + \sum_{i,m} \sum_{\sigma} t_{im}^{\sigma} p_{im}^{\dagger} c_{i\sigma} + \text{h.c.}$$

$$\begin{aligned}
& + \sum_{i,j;\uparrow,\downarrow} t_{ij;\uparrow,\downarrow}^{dd} d_{i,\uparrow,\downarrow}^\dagger d_{j,\uparrow,\downarrow} + \sum_{i,j;m} t_{ij;m}^{pp} p_{i,m}^\dagger p_{j,m} \\
& + \sum_{i,j;\uparrow,\downarrow} t_{ij;\uparrow,\downarrow}^{dp} d_{i,\uparrow,\downarrow}^\dagger p_{j,m} + \text{h.c.} \quad (1)
\end{aligned}$$

where $d_{i,\uparrow,\downarrow}$ is the annihilation operator for Fe-3d electrons with spin \uparrow, \downarrow in the orbital \uparrow, \downarrow at the site i and $p_{i,m}$ is the annihilation operator for As-4p electrons with spin \uparrow, \downarrow in the orbital m at the site i . In eq. (2), the transfer integrals $t_{ij;\uparrow,\downarrow}^{dd}$, $t_{ij;m}^{pp}$, $t_{ij;\uparrow,\downarrow}^{dp}$ and the atomic energies ϵ_i^d , ϵ_m^p are determined so as to fit both the energy and the weights of orbitals for each band obtained from the tight-binding approximation to those from the density functional calculation.²⁸⁾ The doping x corresponds to the number of electrons per unit cell $n = 24 + 2x$ in the present model.

We show the band structure obtained from the d-p tight-binding Hamiltonian eq. (1) together with that obtained from the density functional calculation in the left panel of Fig. 1. It is found that the former reproduces the latter very well. We note that the weights of orbitals also agree very well with each other (not shown). The 10 bands near the Fermi level are mainly constructed by the Fe 3d orbitals and the 6 bands below the 3d 10 bands are mainly constructed by the As 4p orbitals (not shown in Fig. 1). The Fermi surface for the d-p tight-binding model is shown in the right panel of Fig. 1, where we can see nearly circular hole pockets around the Γ point and elliptical

electron pockets around the M point. These results are consistent with the first-principle calculations.^{13,16)}

Now we consider the effect of the Coulomb interaction on Fe site: the intra-orbital (inter-orbital) direct terms U (U^0), the Hund's rule coupling J and the pair-transfer J^0 . Within the RPA,²⁹⁾ the spin susceptibility $\chi^s(q)$ and the charge-orbital susceptibility $\chi^c(q)$ are given in the 50×50 matrix representation as follows,

$$\chi^s(q) = (\hat{1} - \chi^{(0)}(q)\hat{S})^{-1} \chi^{(0)}(q); \quad (2)$$

$$\chi^c(q) = (\hat{1} + \chi^{(0)}(q)\hat{C})^{-1} \chi^{(0)}(q) \quad (3)$$

with the noninteracting susceptibility

$$\chi_{i_1 i_2 i_3 i_4}^{(0)}(q) = \frac{1}{N} \sum_{\mathbf{k}} \sum_{\mathbf{k}'} \frac{f(\epsilon_{\mathbf{k}+\mathbf{q}}) - f(\epsilon_{\mathbf{k}})}{\epsilon_{\mathbf{k}+\mathbf{q}} - \epsilon_{\mathbf{k}}}$$

$$u_{i_1}(\mathbf{k}) u_{i_2}(\mathbf{k} + \mathbf{q}) u_{i_3}(\mathbf{k}) u_{i_4}(\mathbf{k} + \mathbf{q}); \quad (4)$$

where i, j ($= 1-16$) are band indexes, \uparrow, \downarrow ($= A, B$) represent two Fe sites, \uparrow represents Fe 3d orbitals, $u_{i,\uparrow}(\mathbf{k})$ is the eigenvector which diagonalizes H_0 in eq. (1), $\epsilon_{\mathbf{k},i}$ is the corresponding eigenenergy of band i with wave vector \mathbf{k} and $f(\epsilon)$ is the Fermi distribution function. In eqs. (2) and (3), the interaction matrix \hat{S} (\hat{C}) is given by

$$\hat{S} \ (\hat{C}) = \begin{pmatrix} U \ (U) & 0 & 0 & 0 \\ U^0 \ (U^0 + 2J) & 0 & 0 & 0 \\ J \ (2U^0 - J) & 0 & 0 & 0 \\ J^0 \ (J^0) & 0 & 0 & 0 \end{pmatrix} \quad \begin{matrix} (i_1 = i_2 = i_3 = i_4) \\ (i_1 = i_3 \neq i_2 = i_4) \\ (i_1 = i_2 \neq i_3 = i_4) \\ (i_1 = i_4 \neq i_2 = i_3) \end{matrix} : \quad \begin{matrix} 0 \\ 0 \\ 0 \\ 0 \end{matrix} \quad \begin{matrix} (i_1 = i_2 = i_3 = i_4) \\ (i_1 = i_3 \neq i_2 = i_4) \\ (i_1 = i_2 \neq i_3 = i_4) \\ (i_1 = i_4 \neq i_2 = i_3) \end{matrix}$$

In the weak coupling regime, the superconducting gap equation is given by

$$\begin{aligned}
\Delta_{i_1 i_2 i_3 i_4}(\mathbf{k}) &= \frac{1}{N} \sum_{\mathbf{k}^0} \sum_{i_1' i_2' i_3' i_4'} V_{i_1' i_2' i_3' i_4'}(\mathbf{q}) \frac{f(\epsilon_{\mathbf{k}^0, i_1'} + \epsilon_{\mathbf{k}^0, i_2'}) - f(\epsilon_{\mathbf{k}^0, i_3'} + \epsilon_{\mathbf{k}^0, i_4'})}{\epsilon_{\mathbf{k}^0, i_1'} + \epsilon_{\mathbf{k}^0, i_2'} - \epsilon_{\mathbf{k}^0, i_3'} - \epsilon_{\mathbf{k}^0, i_4'}} \\
&\times u_{i_1}(\mathbf{k}^0) u_{i_2}(\mathbf{k}^0) u_{i_3}(\mathbf{k}^0) u_{i_4}(\mathbf{k}^0); \quad (5)
\end{aligned}$$

where $\Delta_{i_1 i_2 i_3 i_4}(\mathbf{k})$ is the gap function and $V_{i_1' i_2' i_3' i_4'}(\mathbf{q})$ is the effective pairing interaction. Within the RPA,²⁹⁾ $V_{i_1' i_2' i_3' i_4'}(\mathbf{q})$ is given in the 50×50 matrix,

$$\hat{V}(\mathbf{q}) = \hat{S} \chi^s(\mathbf{q}) \hat{S} + \frac{1}{2} \hat{S} - \frac{1}{2} \hat{C} \chi^c(\mathbf{q}) \hat{C} - \frac{1}{2} \hat{C}; \quad (6)$$

with $\chi^s = \frac{3}{2}$ for the spin-singlet state and $\chi^c = \frac{1}{2}$ for the spin-triplet state. The gap equation eq. (5) is solved to obtain the gap function $\Delta_{i_1 i_2 i_3 i_4}(\mathbf{k})$ with the eigenvalue λ . At $T = T_c$, the largest eigenvalue λ becomes unity.

In the present paper, we mainly focus on the case with $x = 0.1$, where the superconductivity is observed in the compounds.²⁾ For simplicity, we set $T = 0.02\text{eV}$ and $U = U^0 + 2J$, $J = J^0$. We use 32×32 \mathbf{k} points in the numerical calculations for eqs. (2)–(6), and also use the fast Fourier transformation (FFT) to solve the gap

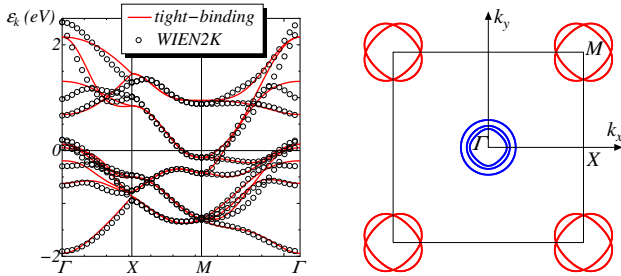


Fig. 1. (Color online) (Left panel) The band structure obtained from eq. (1) (solid line) and that obtained from the density functional calculation (open circle). (Right panel) Fermi surface obtained from the d-p model eq. (1) for $x = 0$

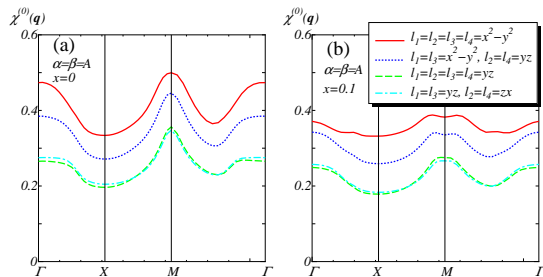


Fig. 2. (Color online) Several components of the noninteracting susceptibility $\chi_{i_1 i_2 i_3 i_4}^{(0)}$ for $x = 0$ (a) and those for $x = 0.1$ (b).

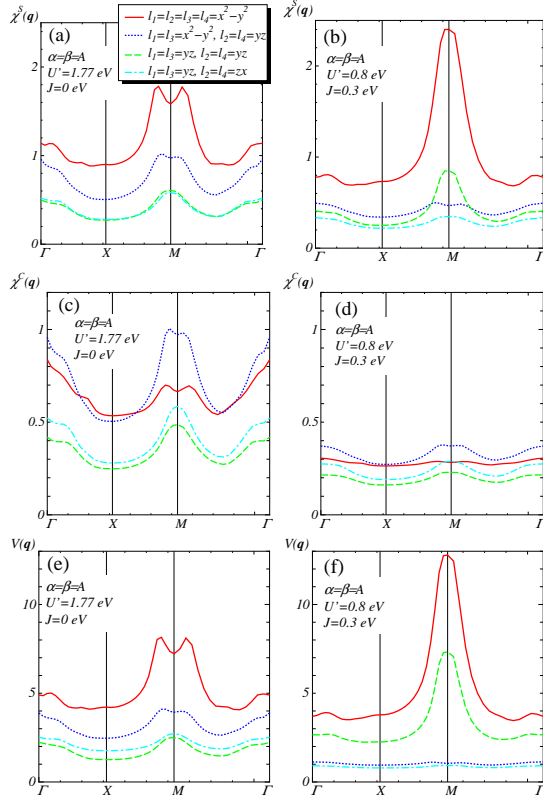


Fig. 3. (Color online) Several components of the spin susceptibility $\chi^s_{\alpha\beta}(q)$ (a) and (b), the charge-orbital susceptibility $\chi^c_{\alpha\beta}(q)$ (c) and (d) and the effective pairing interaction $V_{\alpha\beta}(q)$ (e) and (f), for $U^0 = 1.77$ eV and $J = 0$ eV (a) (c) (e), and for $U^0 = 0.8$ eV and $J = 0.3$ eV (b) (d) (f), respectively.

equation eq. (5).

Fig. 2 shows the several components of the noninteracting susceptibility given in eq. (4) for $x = 0.1$ together with those for $x = 0$ for comparison. We see the peaks centered at the Γ point and those at the M point for $x = 0$, where the former peaks are due to the nesting between the hole (electron) pockets and the latter peaks are due to the nesting between the hole pockets and the electron pockets. With the electron doping, the hole pockets around the Γ point shrink and the smallest one disappears for $x = 0.1$, while the electron pockets become larger (see Fig. 1 of ref. 23). As the result, the nesting effect becomes weak, and then, the peak at the M point is suppressed and shifts around the M point for $x = 0.1$, resulting in the incommensurate SDW as mentioned later.

The several components of the spin susceptibility $\chi^s_{\alpha\beta}(q)$ given in eq. (2) are plotted in Figs. 3 (a) and (b), where the parameters U^0 and J are set to the condition with $x = 1$ (see Fig. 4 (a)). The spin susceptibility is enhanced due to the effect of the Coulomb interaction, especially for the diagonal component of $d_{x^2-y^2}$.

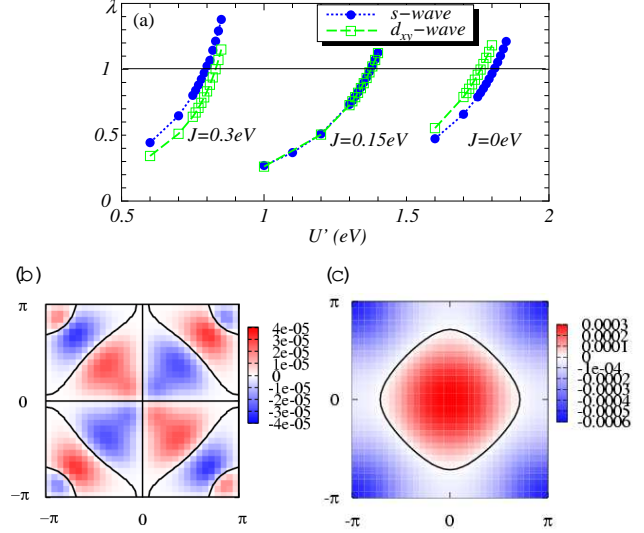


Fig. 4. (Color online) (a) U^0 -dependence of the eigenvalue for $x = 0.1$ and $T = 0.02$ eV. The closed circles and opened squares represent of the s-wave and d_{xy} -wave, respectively. The gap function $V_{\alpha\beta}(q)$ for d_{xy} -wave symmetry at $U^0 = 1.77$ eV; $J = 0$ eV and $x = 0.1$ (b), and that for s-wave symmetry at $U^0 = 0.8$ eV; $J = 0.3$ eV and $x = 0.1$ (c). The solid lines represent the nodes of the gap function.

For $J = 0$ eV, the incommensurate peaks around M point are observed as reflecting the structure of the bare susceptibility shown in Fig. 2 (b). On the other hand, for $J = 0.3$ eV, the commensurate peaks centered at the M point are observed; which is due to an effect of the Hund's coupling J .

The several components of the charge-orbital susceptibility $\chi^c_{\alpha\beta}(q)$ given in eq. (3) are plotted in Figs. 3 (c) and (d). In contrast to the case with the spin susceptibility, the off-diagonal component of $d_{x^2-y^2}$ d_{yz} which corresponds to the orbital susceptibility becomes most dominant due to the effect of the inter-orbital Coulomb interaction U^0 . For $J = 0$ eV, the orbital susceptibility is enhanced and shows peaks around the M point together with those at the Γ point. On the other hand, for $J = 0.3$ eV, the enhancement of the orbital susceptibility is very small, where U^0 is smaller than the intra-orbital interaction $U = U^0 + 2J$ which suppresses the orbital susceptibility.

The several components of the effective pairing interaction $V_{\alpha\beta}(q)$ for the spin-singlet state given in eq. (6) are plotted in Figs. 3 (e) and (f). Since the largest eigenvalue is always spin-singlet state in the present study, we show the effective pairing interaction only for the spin-singlet state. Their structures are similar to those of the spin susceptibility in the both cases for $J = 0$ eV and $J = 0.3$ eV. This is because the contributions of the spin fluctuations to the effective pairing interaction is three times larger than those of the orbital fluctuations according to eq. (6).

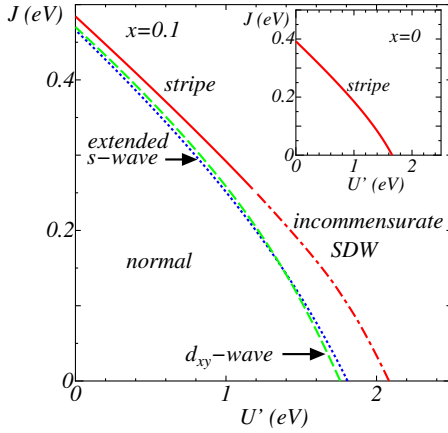


Fig. 5. (Color online) The phase diagram on U^0 - J plane for $x = 0.1$ and $T = 0.02$ eV. The lines represent the instabilities for the stripe antiferromagnetic order (solid), the incommensurate SDW (dot-dashed), the extended s-wave superconductivity (dotted) and the d_{xy} -wave superconductivity (dashed), respectively. The inset shows the magnetic phase diagram for $x = 0$.

Substituting $V_{\lambda_1, \lambda_2, \lambda_3, \lambda_4}(q)$ into the gap equation eq. (5), we obtain the gap function $\Delta_{\lambda}(k)$ with the eigenvalue λ . In Fig. 4 (a), the two largest eigenvalues λ , which are for the extended s-wave and the d_{xy} -wave pairing symmetries, are plotted as functions of U^0 for several values of J . We confirmed that eigenvalues for the other pairing symmetries are much smaller. With increasing U^0 , λ monotonically increases and finally becomes unity at a critical value U_c^0 above which the superconducting state is realized. For $J = 0$ eV, the largest eigenvalue λ is for the d_{xy} -wave symmetry, where the gap function has line nodes on the Fermi surfaces as shown in Fig. 4 (b). On the other hand, for $J = 0.3$ eV, the largest eigenvalue λ is for the extended s-wave symmetry, where the gap function changes its sign between the hole pockets and the electron pockets without nodes on the Fermi surfaces as shown in Fig. 4 (c).^{17,19,20} For $J = 0.15$ eV, these two eigenvalues are almost degenerate. The extended s-wave pairing is mediated by the pairing interaction with the sharp peak at $Q = (\pi, \pi)$ (see Fig. 3 (f)), while the d_{xy} -wave pairing is mediated by the pairing interaction with the incommensurate peaks around $Q = (\pi, \pi)$ together with the peak at $Q = (0, 0)$ (see Fig. 3 (e)).

The phase diagram on U^0 - J plane for $x = 0.1$ and $T = 0.02$ eV is shown in Fig. 5, where the magnetic instability is determined by the divergence of the spin susceptibility and the superconducting instability is determined by $\lambda = 1$ as mentioned before. For $J > 0.25$ eV, the stripe-type antiferromagnetic order with $Q = (\pi, \pi)$ appears, while, for $J < 0.25$ eV, the incommensurate SDW (ISDW) with $Q = (\pi, \pi)$ appears (see also Figs. 3 (a) and (b)). It is noted that we only observe the stripe-type antiferromagnetic order for $x = 0$ as shown in the inset in Fig. 5. The extended s-wave pairing is realized near

the stripe-type antiferromagnetic order for $J > 0.15$ eV, where the spin fluctuation with $Q = (\pi, \pi)$ is enhanced as shown in Fig. 3 (b). On the other hand, the d_{xy} -wave pairing is realized near the ISDW for $J < 0.15$ eV, where the spin fluctuation with $Q = (\pi, \pi)$ is enhanced as shown in Fig. 3 (a).

In summary, we investigated the pairing symmetry of the two-dimensional 16-band d-p model by using the RPA and obtained the phase diagram on the U^0 - J plane for $x = 0.1$; $T = 0.02$ eV. For $J > 0.15$ eV, the most favorable pairing is extended s-wave symmetry whose order parameter changes its sign between the hole pockets and the electron pockets, while for $J < 0.15$ eV, it is d_{xy} -wave symmetry. Then, the effect of the Hund's coupling J is crucial to realize the extended s-wave pairing in the pure system without impurities. According to the recent experiment of very weak T_c -suppression by Co-impurities,⁶⁾ we suppose that the d_{xy} -wave pairing is suppressed by pair breaking effect and the extended s-wave pairing is realized in real materials.³⁰⁾

Acknowledgment

The authors thank M. Sato, H. Kontani and K. Kuroki for useful comments and discussions. This work was partially supported by the Grant-in-Aid for Scientific Research from the Ministry of Education, Culture, Sports, Science and Technology.

- 1) Y. Kamihara et al.: J. Am. Chem. Soc. 128 (2006) 10012.
- 2) Y. Kamihara et al.: J. Am. Chem. Soc. 130 (2008) 3296.
- 3) Z. A. Ren et al.: Chin. Phys. Lett. 25 (2008) 2215.
- 4) C. Cruz et al.: Nature 453 (2008) 899.
- 5) K. Matano et al.: Europhys. Lett. 83 (2008) 57001.
- 6) A. Kawabata et al.: J. Phys. Soc. Jpn. 77 (2008) 103704.
- 7) K. Hashimoto et al.: arXiv/0806.3149.
- 8) G. Mu et al.: Chin. Phys. Lett. 25 (2008) 2221.
- 9) H. Liu et al.: arXiv/0806.4806.
- 10) H. Ding et al.: arXiv/0807.0419.
- 11) T. Kondo et al.: arXiv/0807.0815.
- 12) Y. Nakai et al.: J. Phys. Soc. Jpn. 77 (2008) 073701.
- 13) D. J. Singh et al.: Phys. Rev. Lett. 100 (2008) 237003.
- 14) K. Haule et al.: Phys. Rev. Lett. 100 (2008) 226402.
- 15) G. Xu et al.: Europhys. Lett. 82 (2008) 67002.
- 16) L. Boeriet al.: Phys. Rev. Lett. 101 (2008) 026403.
- 17) I. I. Mazin et al.: Phys. Rev. Lett. 101 (2008) 057003.
- 18) K. Seo et al.: arXiv/0805.2958.
- 19) K. Kuroki et al.: Phys. Rev. Lett. 101 (2008) 087004.
- 20) T. Nomura: arXiv/0807.1168.
- 21) F. Wang, et al.: arXiv/0805.3343; arXiv/0807.0498.
- 22) Z. Yao, et al.: arXiv/0804.4166.
- 23) Y. Yanagi, Y. Yamakawa and Y. Ono: arXiv/0808.1192.
- 24) J. P. Perdew, et al.: Phys. Rev. Lett. 77 (1996) 3865.
- 25) P. B. Laha et al.: WIEN 2k, An Augmented Plane Wave + Local Orbitals Program for Calculating Crystal Properties (Technische Universität Wien, 2002, Austria); <http://www.wien2k.at>
- 26) T. Nomura et al.: arXiv/0804.3569.
- 27) V. Cvetkovic et al.: arXiv/0804.4678.
- 28) Y. Yamakawa, Y. Yanagi and Y. Ono in preparation.
- 29) T. Takimoto et al.: Phys. Rev. B 69 (2004) 104504.
- 30) Y. Senga et al.: arXiv/0809.0374.